

Highly Stable and Eco-friendly Marine Self-Charging Power Systems Composed of Conductive Polymer Supercapacitors with Seawater as an Electrolyte

Baofeng Zhang, Chuguo Zhang, Wei Yuan, Ou Yang, Yuebo Liu, Lixia He, Yuexiao Hu, Linglin Zhou, Jie Wang,* and Zhong Lin Wang



Cite This: <https://doi.org/10.1021/acsami.1c22129>



Read Online

ACCESS |



Metrics & More



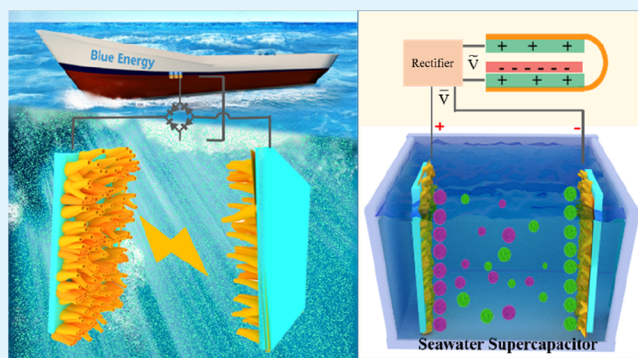
Article Recommendations



Supporting Information

ABSTRACT: A self-charging power system harvesting random and low-frequency wave energy into electricity provides a promising strategy for the construction of smart oceans. However, the system faces huge challenges of easy corrosion in the marine environment and the utilization of toxic organic electrolytes in energy storage devices. To address the issues above, a seawater supercapacitor (SWSC) for the marine self-charging power system is rationally proposed by using a conductive polymer, polypyrrole with hollow morphology (h-PPy), to enhance the stability and capacitance while using seawater as an eco-friendly electrolyte to reduce the cost and achieve sustainability. The hollow design provides a shortcut for the ion transportation of seawater into the h-PPy electrode, and the SWSC achieves a high power density of 4.32 kW kg^{-1} under an energy density of 5.12 W h kg^{-1} . Even after 180 days in seawater, h-PPy still endows a mass retention of 99.9%, enabling the SWSC to maintain a stability of 99.3% after 6000 cycles. More importantly, when combined with a TENG module as the marine self-charging power system to harvest wave energy, the system provides a stable output in water wave to drive electronics and sensors, which shows a competitive potential in the smart ocean and marine internet of things.

KEYWORDS: marine self-charging power system, conductive polymer supercapacitor, triboelectric nanogenerator, seawater electrolyte, low-cost and eco-friendly



INTRODUCTION

Monitoring devices and sensors that allow for detecting temperature and pressure, measuring force and acceleration, locating ships and cargoes, and so forth, are indispensable parts for the development of marine internet of things (IoT) and smart oceans.^{1,2} With billions to trillions of sensors distributed in the ocean, developing a self-powered manner with continuous, sustainable, and pervasive features from water waves is a unique approach to power these devices.^{3–5} Compared with electromagnetic generators (EMGs) that need high frequencies, triboelectric nanogenerators (TENGs) coupled with electrification and electrostatic induction can be utilized to efficiently convert random and low-frequency wave energy into electricity in the ambient environment.^{6–8} In principle, the TENG can be viewed as an alternating current (AC) power supply in series with a varying capacitor,^{9–11} the outputs of which are usually irregular and not suitable for directly driving conventional electronics. Thus, a TENG-based self-charging power system containing an energy storage device to *in situ* store the electricity and provide a stable direct current (DC) input is severely required, which would reduce the need

for an external power source, enhance the portability, and eliminate the inconveniences of recharging and replacing energy storage devices.^{12,13}

To sufficiently harvest the water wave energy, a series of self-charging power systems based on TENG, including the spherical-shaped TENG,¹⁴ arc-shaped TENG,¹⁵ water balloon TENG,¹⁶ stacked pendulum-structured TENG,¹⁷ and even hybrid TENG with EMG devices,¹⁸ is designed to charge the energy storage devices to drive active sensing devices in the fields of chemical and environmental monitoring, smart ocean, and so forth.^{7,19–21} However, most of the energy storage devices utilized are supercapacitors (SCs) and batteries with organic mechanicals as electrolytes to enhance the energy density.^{22–24} Usually, these electrolytes are toxic and

Received: November 17, 2021

Accepted: January 28, 2022

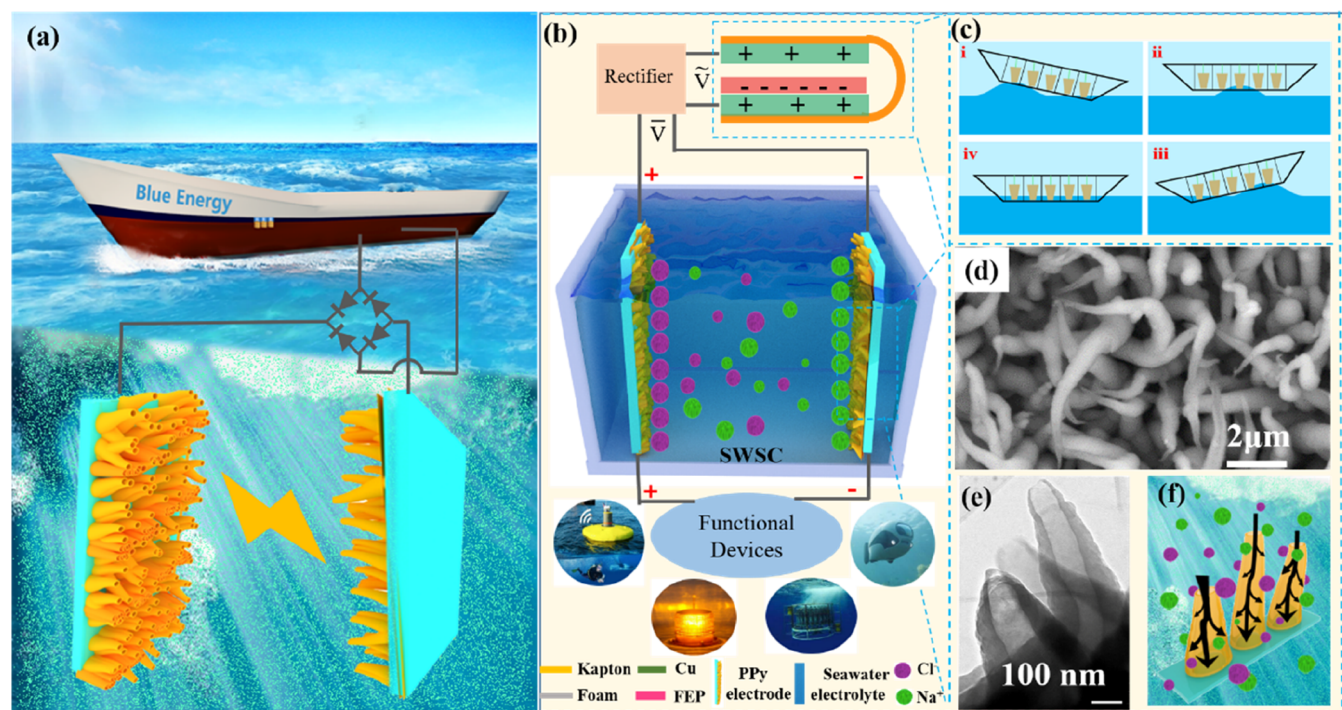


Figure 1. Structural design and working mechanism of the marine self-charging power system. (a) Marine self-charging power system composed of the vessel with the integrated BM-TENG module and h-PPy SWSC with natural seawater as the electrolyte. (b) Device configuration of the marine self-charging power system by harvesting the water wave energy and in situ h-PPy SWSC for driving electricity. (c) Working principle of the vessel with integrated BM-TENG modules in water waves [a wave moves to (i) the left, (ii) middle, and (iii) right sides of a vessel, and (iv) the wave leaves the vessel]. (d) SEM image, (e) TEM image of the as-prepared horn-like PPy electrode in the h-PPy SWSC, and (f) hollow morphology of the horn-like PPy facilitating the transportation of Na^+ and Cl^- into the active materials.

unaffordable, which impedes the commercial application of SCs. As an alternative, aqueous electrolytes have been extensively studied owing to their intrinsic characteristics of high ionic conductivity, easy operating procedures, and so on.^{22,25–27} However, the adopted electrolytes are mainly strong acid electrolytes and strong alkali electrolytes, which will severely corrode the active materials and substrates. More importantly, these organic electrolytes and aqueous electrolytes would pose a huge threat to marine organisms when leaked into the marine environment.²⁸ In such circumstances, mild electrolytes have been attracting increasing attention. Natural seawater with a salinity of around 3.5% (i.e., 0.6 M NaCl²⁹) is considered as a good, mild, and eco-friendly electrolyte.^{30,31} Besides, the employment of seawater at zero cost would reduce the cost of SCs significantly and further improve the self-power system distinctly for commercial implementations. Although several SCs adopt activated carbon fibers,²² MXene,³² and transition metal oxides and their composites³³ as active materials with seawater as an electrolyte to store the energy harvested from TENG, the research studies on the utilization of natural seawater are limited due to the mismatching between the active materials and the ions in seawater.

On the other hand, polypyrrole (PPy), especially micro/nano structured PPy, is one of the most promising pseudocapacitive electrode materials because of its greater density and better degree of flexibility than most other conducting polymers.³⁴ Its high electrical conductivity will definitely lead to significantly improved electron transport and the ability to undergo a fast redox reaction to store charge. In addition, the merits of easy synthesis, environmental compatibility, and thermal and chemical stability promote

PPy to be used in the SC. However, few studies have reported the mechanism of PPy as an active material to store the energy from TENG with seawater as an electrolyte.

Herein, a marine self-charging power system consisting of a seawater supercapacitor (SWSC) and a TENG module is proposed to provide a stable output for the electronics. For the SWSC, a conductive polymer, hollow PPy, is prepared as an electrode to enhance the stability and capacitance, while seawater is employed as an eco-friendly aqueous electrolyte to reduce the cost and achieve sustainability. With the hollow design, the h-PPy electrode facilitates the ions of seawater to transport into the electrode, and the SWSC achieves a high power density of 4.32 kW kg^{-1} under an energy density of 5.12 W h kg^{-1} . Even after aging in seawater for 180 days, h-PPy still endows mass retention of 99.9%, enabling the SWSC to maintain stability of 99.3% after 6000 cycles. More importantly, when combined with the TENG module, which delivers a power density of nearly 200 W m^{-3} , the assembled marine self-charging power system provides a DC output to drive electronics and sensors, which shows competitive potential in the smart ocean and marine IoTs.

RESULTS AND DISCUSSION

Structural Design and Working Mechanism. In order to realize the effective development and utilization of water wave energy, we designed a marine self-charging power system (Figure 1a), which mainly consists of a vessel platform, a TENG module, and an *in situ* SWSC. With the good maneuverability and stable environment of a vessel, a vessel with an integrated TENG module can be deployed easily in the ocean to harvest the ocean wave and harbor it back to avoid

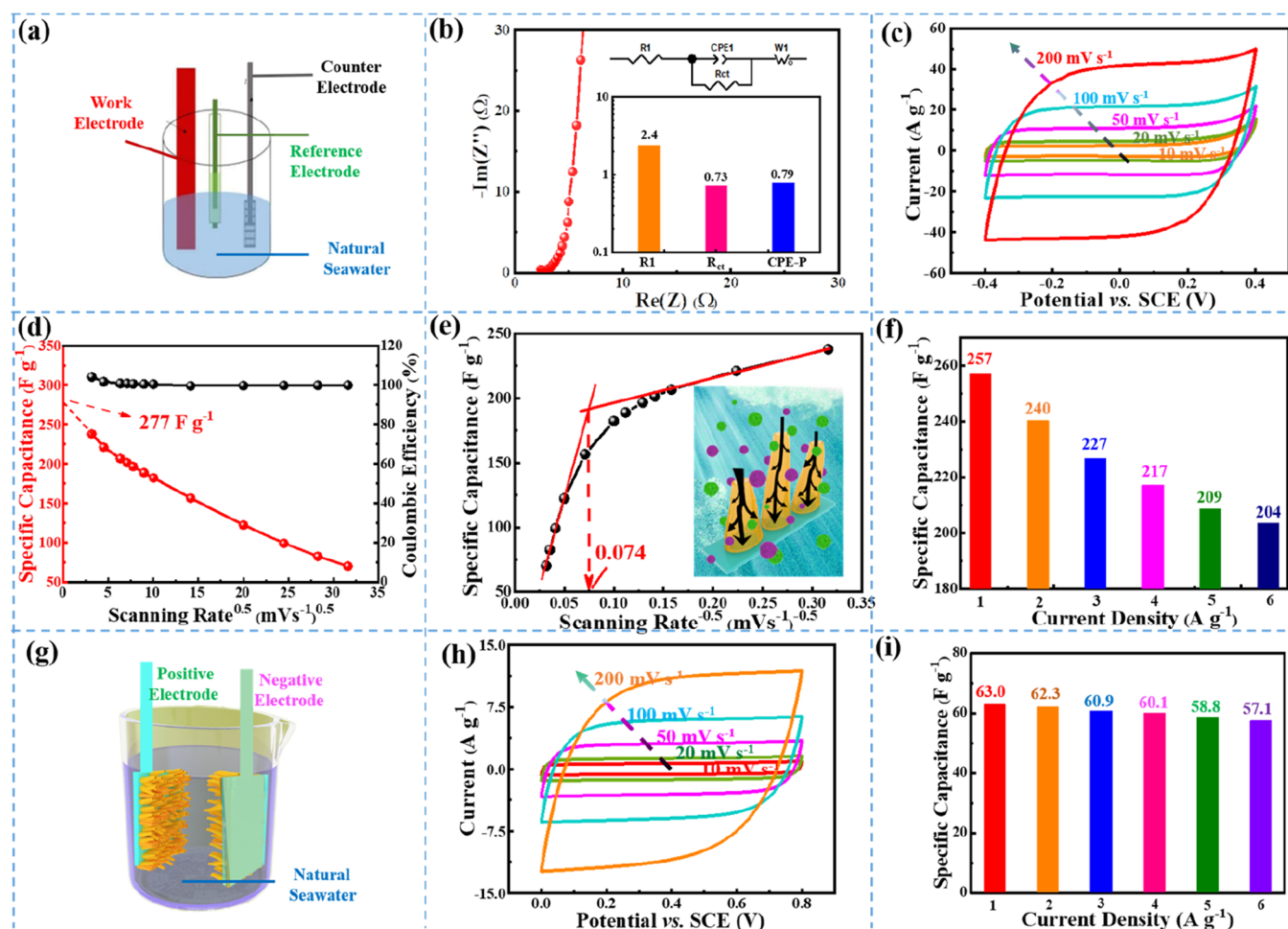


Figure 2. Electrochemical performances of h-PPy SWSCs. (a) Schematic structure, (b) EIS curve, (c) different scan rates of CV curves at -0.4 to 0.4 V, (d,e) specific capacitance normalized with respect to the scanning rate plotted as a function of the square root of the sweep rate and the inverse square root of the sweep rate, (f) specific capacitance at different current densities of the h-PPy electrode in a three-electrode system with seawater as the electrolyte. (g) Schematic structure, (h) CV curve, and (i) specific capacitance of the electrode calculated from GCD.

the extreme environment.³⁵ The hollow seawater SWSC can efficiently store electricity from TENG by employing seawater as an eco-friendly aqueous electrolyte to reduce the cost and achieve sustainability. Then, the marine self-charging power system can be utilized to drive the active sensing devices and devices in the marine environment with a DC output (Figure 1b). As illustrated in Figure S1a, the TENG module is composed of a bracket, a bifilar-pendulum, and two multilayer-structured TENGs (M-TENG). M-TENG is fabricated using a zigzag Kapton substrate, foams for increased contact, copper foil electrodes, and a dielectric layer-fluorinated ethylene propylene film (FEP) with a thickness of $30 \mu\text{m}$ (Figure S1b). In principle, when a wave moves to the left side of a vessel (Figure 1c-i), the left bow of the vessel rises up and the bifilar-pendulum shifts to the right to push the right copper foil in contact with the left FEP film. Owing to triboelectric effects, the Cu electrode with low electronegativity exhibits a positive charge and the FEP film, a negative one (Figure S1c-i). As the waves move to the middle of the vessel, the middle of the vessel rises up and the whole vessel tends to be in a horizontal direction (Figure 1c-ii). The bifilar-pendulum swings back to the vertical state, and the positive charge flows from the left Cu electrode to the right one by external circuit (Figure S1c-ii). Next, as the wave moves to the right side of the vessel, the left bow falls down and the right bow rises up to push the bifilar-

pendulum to the right. Then, the left Cu electrode separates from the right FEP dielectric layer completely (Figure 1c-iii), and all the positive charges flow to the right Cu electrode (Figure S1c-iii). As the waves leave, the vessel and the bifilar-pendulum swing back to the initial state (Figure 1c-iv). Moreover, the positive charges transfer from the right Cu electrode to the left one, generating a reverse current in the external circuit (Figure S1c-iv). In addition to better understanding the operative principle of the M-TENG unit, the corresponding electric potential distribution under different states is simulated by COMSOL, which shows the ability of the gain and loss electrons and the theoretical maximum voltage output of ~ 600 V (Figure S2). It is notable that the M-TENGs on the left and right work in opposite phases, and an AC current with a pulse signal is generated. Thus, it is severely required to convert the irregular AC current into stable DC input power for driving conventional electronics.

In order to *in situ* store the energy from the TENG module above, the SWSC with hollow PPy as an electrode to enhance the stability and capacitance, while seawater as an eco-friendly aqueous electrolyte to reduce the cost is proposed. As a conductive polymer, PPy can exhibit a stable performance in the marine environment. Besides, with the assistance of electrochemical preparation, it is closely adhered to the substrate to ensure high specific capacitance, fast charging/

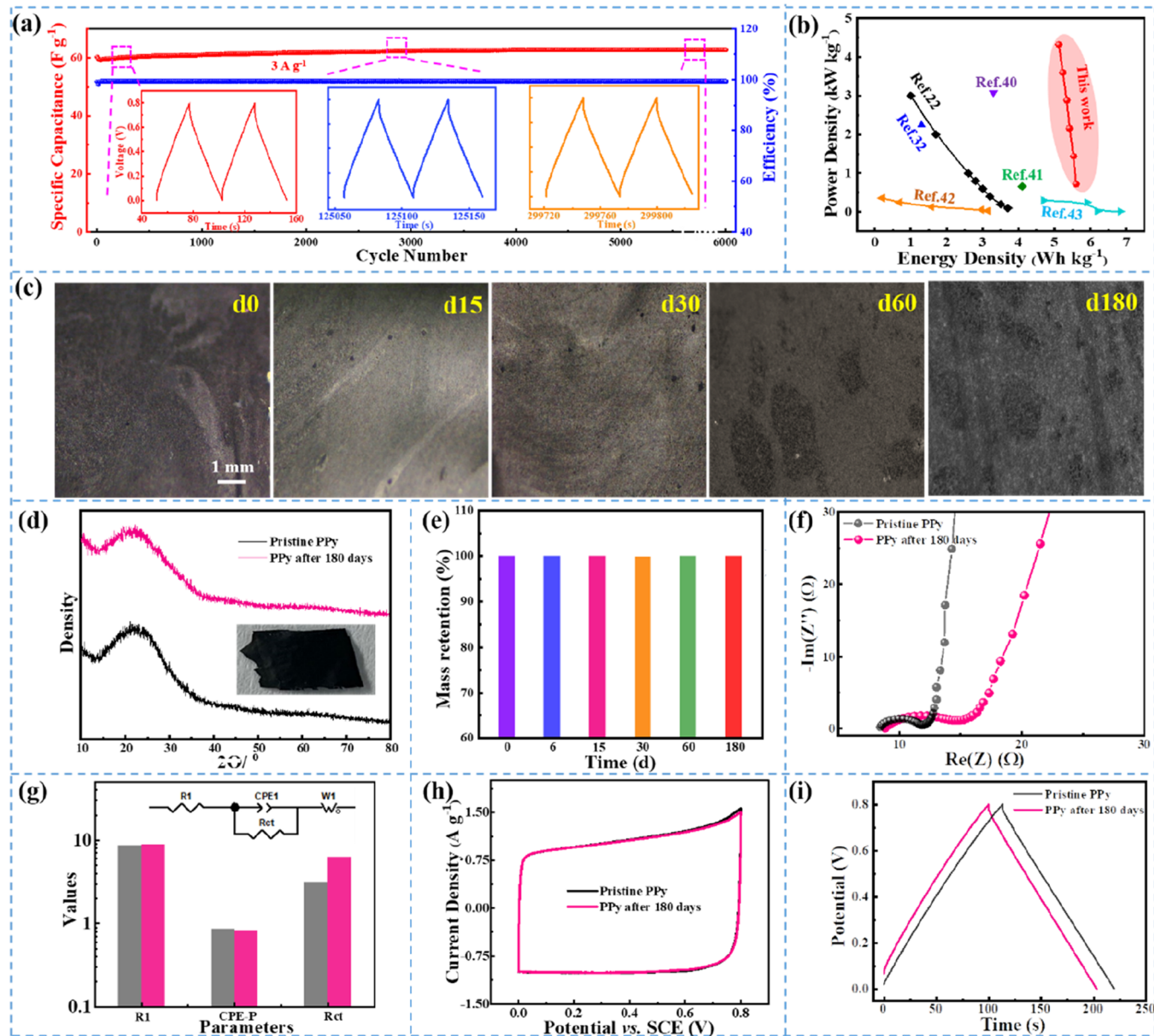


Figure 3. Stability and aging tests of the SWSC in seawater. (a) Stability retention and (b) Ragone plots of power density as a function of energy density of the h-PPy SCs in a two-electrode system in seawater. (c) OM images of the h-PPy films on the electrode in seawater, (d) XRD tests, (e) mass retention, (f) EIS curve and the fitting results, (h) CV curve, and (i) GCD curves of the SWSC after h-PPy electrode immersion in seawater for 180 days.

discharging ability, and capacitance retention, while avoiding the conductive agent and binder. As shown in Figure 1d, the as-prepared PPy is grown densely and homogeneously, overlapping with each other with an average length of 10 μm . The TEM images further suggest that the pore diameter of hollow PPy is 100 nm (Figure 1e), which would provide extra surface area to increase the capacitance. Besides, the hollow morphology creates a high way for the transportation of ions (mainly Na^+ and Cl^-) of natural seawater in the electrode, facilitating the exchange of ions and electrons in the active material (Figure 1f). As a result, the as-prepared SWSC would exhibit a large specific capacitance and a high power density.

Electrochemical Performance of h-PPy SWSCs. As an indispensable part, the performance of the SC would greatly influence the output of the marine self-charging power system. The electrochemical performances of the as-prepared PPy

electrode are first tested in a three-electrode system, where the PPy electrode, the platinum foil, and the saturated calomel electrode (SCE) serve as the working electrode, counter electrode, and reference electrode, respectively, with natural seawater as the electrolyte (Figure 2a). The electrochemical impedance spectroscopy (EIS) suggests that the inherent resistance (R_1) at high frequency and charge transfer resistance (R_{ct}) at middle frequency of the h-PPy electrode are 2.4 and 0.73 Ω , respectively (Figure 2b), indicating not only a low resistance between the current collector and active materials but also a high electron-ion exchange ability between active materials and the electrolyte. It also demonstrates that the ions in the natural seawater electrolyte can be transported efficiently in the PPy. Besides, the fitting parameter CPE-P (0.79) and the Bode phase angle plot (Figure S3) show that the phase angle at the tail is about -84.9° (very close to that of an ideal

capacitor, -90°), which further highlights the ideal capacitive nature of the h-PPy electrode in the seawater. The cyclic voltammetry (CV) test (Figure S4) at a scan rate of 10 mV s^{-1} suggests that the rational potential window for the PPy electrode is -0.4 to 0.4 V due to the polarization effect at higher potential. The symmetrical CV curve also shows that the PPy electrode is a promising candidate for symmetric SCs. In order to verify fast charging/discharging ability, the CV curves at different scan rates ($10, 20, 50, 100,$ and 200 mV s^{-1}) are conducted, which shows that the PPy electrode can work normally even at a high scan rate of 200 mV s^{-1} because of the quasi-rectangular profiles (Figure 2c). Figure 2d indicates that the theoretical specific capacitance of h-PPy is as high as 277 F g^{-1} , obtained from the intersection point of the extension cord of the specific capacitance curve and y axis. In addition, it further suggests that the as-prepared PPy electrode enables the specific capacitances of $237.7, 221.2, 201.4, 182.5,$ and 156.5 F g^{-1} under the scan rates of $10, 20, 50, 100,$ and 200 mV s^{-1} , respectively, which are close to the above calculated theoretical specific capacitance.

In order to further characterize the h-PPy electrode, an apparent diffusion coefficient (D) is proposed in Figure 2f according to eq 1 below^{36,37}

$$D = h^2/\tau \quad (1)$$

where h is the thickness of the film and τ is the time constant obtained from the eq 2

$$\tau = V_m/V_c \quad (2)$$

where V_m is the potential window obtained from the CV (0.8 V) and V_c is calculated from the intersection point of two lines with different slopes, as shown in Figures 2f and S5.

As a result, the calculated apparent diffusion coefficient for the h-PPy electrode ($D_{\text{h-PPy}}$) is $9.25 \times 10^{-9} \text{ cm}^2 \text{ s}^{-1}$. Compared with the diffusion coefficient of conventional cauliflower-like PPy (Figure S6), which is $6.54 \times 10^{-9} \text{ cm}^2 \text{ s}^{-1}$, the results suggest that the hollow structure of h-PPy facilitates the diffusion rate of counterions in seawater.

The galvanostatic charging/discharging test (GCD) further displays the fast charging/discharging ability of the as-prepared h-PPy electrode at a current load of $1, 2, 3, 4, 5,$ and 6 A g^{-1} ($330, 660, 1000, 1330, 1660,$ and $2000 \mu\text{A}$, respectively) (Figure S7). The charging and discharging curves of the h-PPy electrode are symmetric and linear in the entire range of potential without any obvious ohm-drop (IR -drop), suggesting a fully reversible electrochemistry and ideal capacitance behavior. The specific capacitances are as high as $257, 240, 227, 217, 209,$ and 204 F g^{-1} at the current load of $1, 2, 3, 4, 5,$ and 6 A g^{-1} (Figure 2f), respectively, which is in accordance with the results from CV.

The applicability of the symmetric seawater SC (SWSC) composed of two h-PPy electrodes is evaluated in a two-electrode system with natural seawater as the electrolyte (Figure 2g). The EIS curves of the h-PPy SWSC suggest that the inherent resistance (R_1) at high frequency, the charge transfer resistance (R_{ct}) at middle frequency, and the diffusion parameter (CPE-P) at low frequency are $8.5 \Omega, 3.1 \Omega,$ and 0.86Ω , respectively (Figure S8a). The Bode phase angle plot (Figure S8b) further shows that it exhibits an ideal capacitive nature of the h-PPy SWSC owing to the high phase angle at the tail of -85.8° . The CV curves conducted at different scan rates of $10, 20, 50, 100,$ and 200 mV s^{-1} indicate that the SWSC acquires fast charging/discharging ability even at a high

scan rate of 200 mV s^{-1} owing to the quasi-rectangular profiles (Figure 2h). GCD curves further suggest that the SWSC can work under the high current densities of $1, 2, 3, 4, 5,$ and 6 A g^{-1} ($660, 1332, 2000, 2660, 3320,$ and $4000 \mu\text{A}$, respectively) (Figure S9), where the corresponding specific capacitances of the electrode in the SWSC are $63.0, 62.3, 60.9, 60.1, 58.8,$ and 57.1 F g^{-1} (Figure 2i).

Stability and Aging Tests of SWSCs in Seawater.

Natural seawater, compared with the previous strong aqueous acid electrolyte and alkali electrolyte, is considered as a mild and eco-friendly electrolyte with zero cost. In addition, the stability of the electrode in seawater will severely affect the electrochemical performance of the SCs. The symmetric SWSC assembled by the PPy electrode obtains the stability of 99.3% after 6000 cycles with the specific capacitance of 60.1 F g^{-1} at the current density of 3 A g^{-1} (Figure 3a). The reason mainly lies in two aspects: (1) the Ti film as the current collector in the electrode is more stable than the commonly used current collectors such as Al and Cu films. As shown in Figure S10, the optical morphology (OM) of the samples in seawater indicates that the corrosion of samples becomes serious with increase in time. For the Cu electrode, the corrosion signs of pits are observed on the surface of the sample on day 15. Moreover, the density of pits increases significantly on days 30, 60, and 180. Besides, the corroded bands and cracks also appeared within the local area on days 60 and 180, respectively, suggesting that serious corrosion was generated (Figure S10a). Compared with the Cu electrode, the OM images of the Al electrode illustrate a relatively lower density of pits (Figure S10b). However, the size of the pits is roughly 0.5 mm (day 30) to 1 mm (day 60), which is far larger than that of the Cu electrode. Although the pits are deepened and corroded bands are observed on day 180, it seems that the corrosion resistance of the Al electrode is better than the Cu electrode due to no appearance of cracks. The OM images of the Ti electrode indicate that the electrode is pretty stable without the observation of pits or corroded bands even after 180 days of immersion in seawater (Figure S10c).

The whole images of the samples after immersion in seawater for 180 days suggest that clear cracks are observed on the Cu electrode, while a corrosive layer is found on the Al electrode. On the contrary, the Ti electrode maintains a relatively stable state (Figure S10d). The results are also supported by the mass retention rate curves, which suggest that the mass of the Cu electrode decreases from 100% at the initial state to 76.8% at day 180, while the mass of the Al electrode decreases from 100% to 86.4% . On the contrary, the Ti electrode appears to have a stable mass retention rate of about 100% even after immersion in seawater for 180 days (Figure S10e). The X-ray diffraction (XRD) curves show that Cu_2O and $\text{Cu}(\text{OH})\text{Cl}$ are generated in the Cu electrode due to the existence of H_2O and Cl^- in seawater (Figure S10f). For the Al electrodes, although no new compound is found, the (002) lattice plane is missing after corrosion which suggests that the (002) lattice plane is prone to be corroded (Figure S10g). For Ti, one of the most stable materials, the structure is seldom changed (Figure S10g), which is indicative of stable performance and anti-corrosion ability in seawater.

The stability of symmetric SWSC is also derived from the high stability of PPy. At the molecular scale, the band energy of the C–C bond, C–N bond, and C–H bond in the PPy is high enough that they can hardly be broken in seawater. At the chain scale, the high stability of the PPy is attained due to the

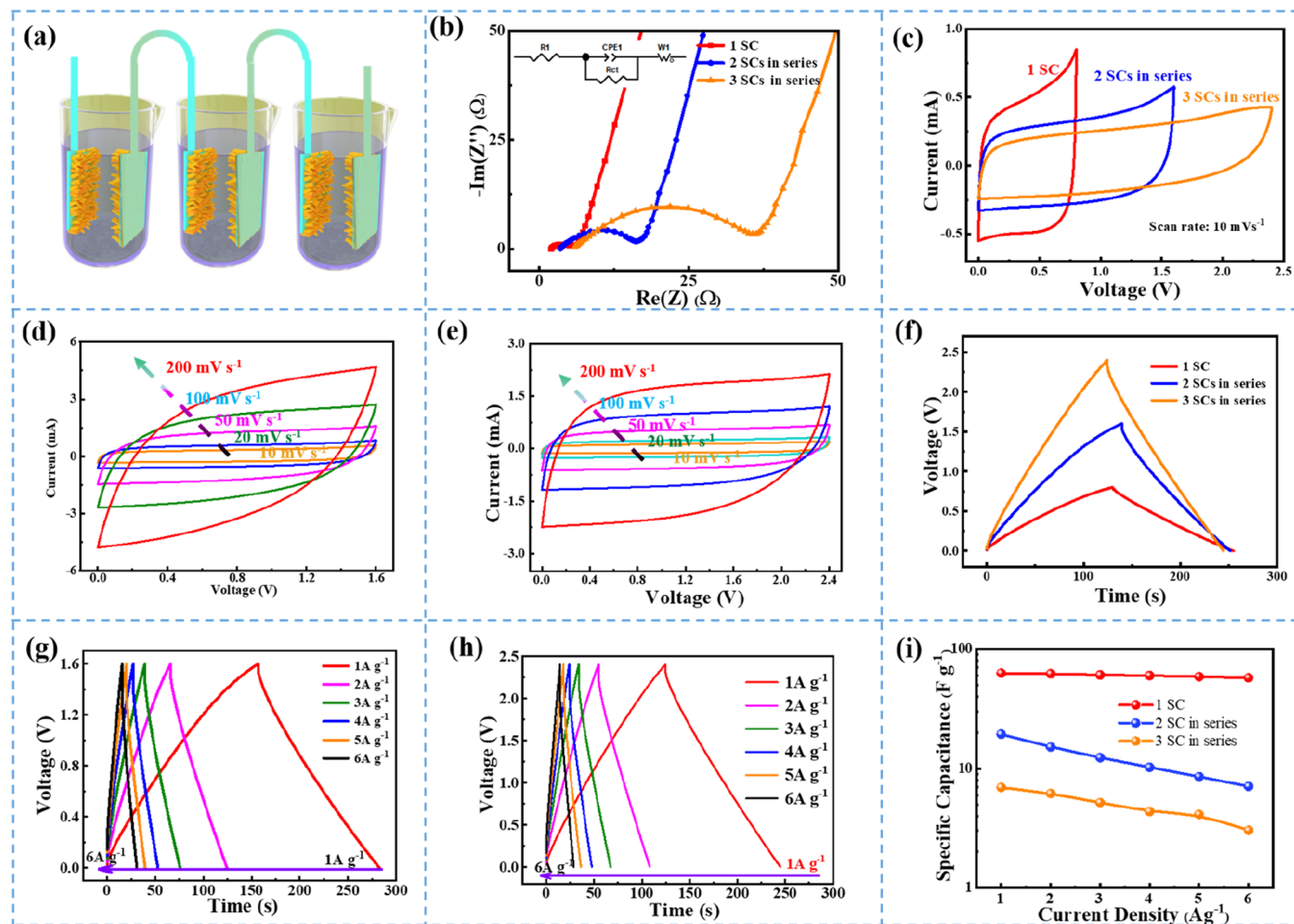


Figure 4. Electrochemical performance of h-PPy SWSCs in series. (a) Schematic structure, (b) EIS curve, (c) potential window test from CV at the scan rate of 10 mV s^{-1} , (d,e) different scan rates of CV curves when two and three h-PPy SWSCs are in series, (f) GCD curves at 1 A g^{-1} , (g,h) GCD curves at different current densities when two and three h-PPy SWSCs are in series, and (i) specific capacitance calculated from GCD for h-PPy SWSCs in series with the increase in h-PPy SC units.

closure of the polymeric entanglement during the electrochemical treatment, which hinders oxygen diffusion through the polymer.³⁸ At the bulk scale, the polymer films prepared at low potentials have the best characteristics in terms of their conductivity, stability, chemical reversibility, and chain length due to slow growth kinetics.³⁹

Taking these advantages, the SWSC delivers a considerable power density of 4.32 kW kg^{-1} at an energy density of 5.12 Wh kg^{-1} (Figure 3b), which outperforms the seawater electrolyte-based devices reported to date, including the activated carbon fiber symmetric SC (3.0 kW kg^{-1} @ 1.0 Wh kg^{-1}),²² V_2CT_x MXene symmetric SC (30 W kg^{-1} @ 3.14 Wh kg^{-1}),³² and $\text{Ti}_3\text{C}_2\text{T}_x$ MXene symmetric SC (15 W kg^{-1} @ 6.83 Wh kg^{-1}).⁴⁰ These values are also higher than those of transition metal oxide-based SCs previously reported in the aqueous electrolyte, such as carbon nanotubes @Mn-MOF symmetrical SC (1.3 kW kg^{-1} @ 2.2 Wh kg^{-1}),⁴¹ MnO_2 , Fe_3O_4 , and V_2O_5 SC (3.3 kW kg^{-1} @ 3.08 Wh kg^{-1}),⁴² and polyaniline/MnO₂/graphene//porous graphene asymmetric SC (4.1 kW kg^{-1} @ 0.66 Wh kg^{-1}).⁴³ Although some works with transition metal oxides/carbon nanotube composites as active materials exhibit higher energy density and power density,^{33,44} stability needs to be further improved (Table S1).

The aging test of h-PPy is conducted by immersion of the h-PPy electrode in natural seawater for 180 days at room

temperature. The optical microscopy (OM) images of the PPy electrode indicate that the PPy electrode is pretty stable without the observation of pits or corroded bands even after 180 days of immersion in seawater (Figure 3c). Although the pH values of seawater after immersion of the PPy electrode drop slightly from 8.24 to 7.86 due to the transfer of *p*-toluenesulfonic acid (TOSH) in the active material when preparing PPy into seawater (Figure S11), the structure of PPy is seldom changed (Figure 3d), which is indicative of its stable performance and anti-corrosion ability in seawater. The results are also supported by the mass retention curves, which suggest that the PPy electrode exhibits almost 100% even after immersion in seawater for 180 days (Figure 3e).

After assembling the aged h-PPy electrode into the symmetric SWSC, the EIS curves suggest that the inherent resistance (R_1) at high frequency, the charge transfer resistance (R_{ct}) at middle frequency, and the diffusion parameter (CPE-P) at low frequency of the h-PPy SWSC are respectively 8.8Ω , 6.2Ω , and 0.81Ω , which are slightly larger than those of the pristine at 8.5Ω , 3.1Ω , and 0.86Ω (Figure 3f,g). As reported, the considerable increase in the charge transfer and diffusion resistance is mainly attributed to the corrosion of the substrate in the electrode by the impact of Cl^- ions present in seawater electrolyte.⁴⁵ However, the current collector used in this article is a Ti foil, which is more stable in the seawater electrolyte.

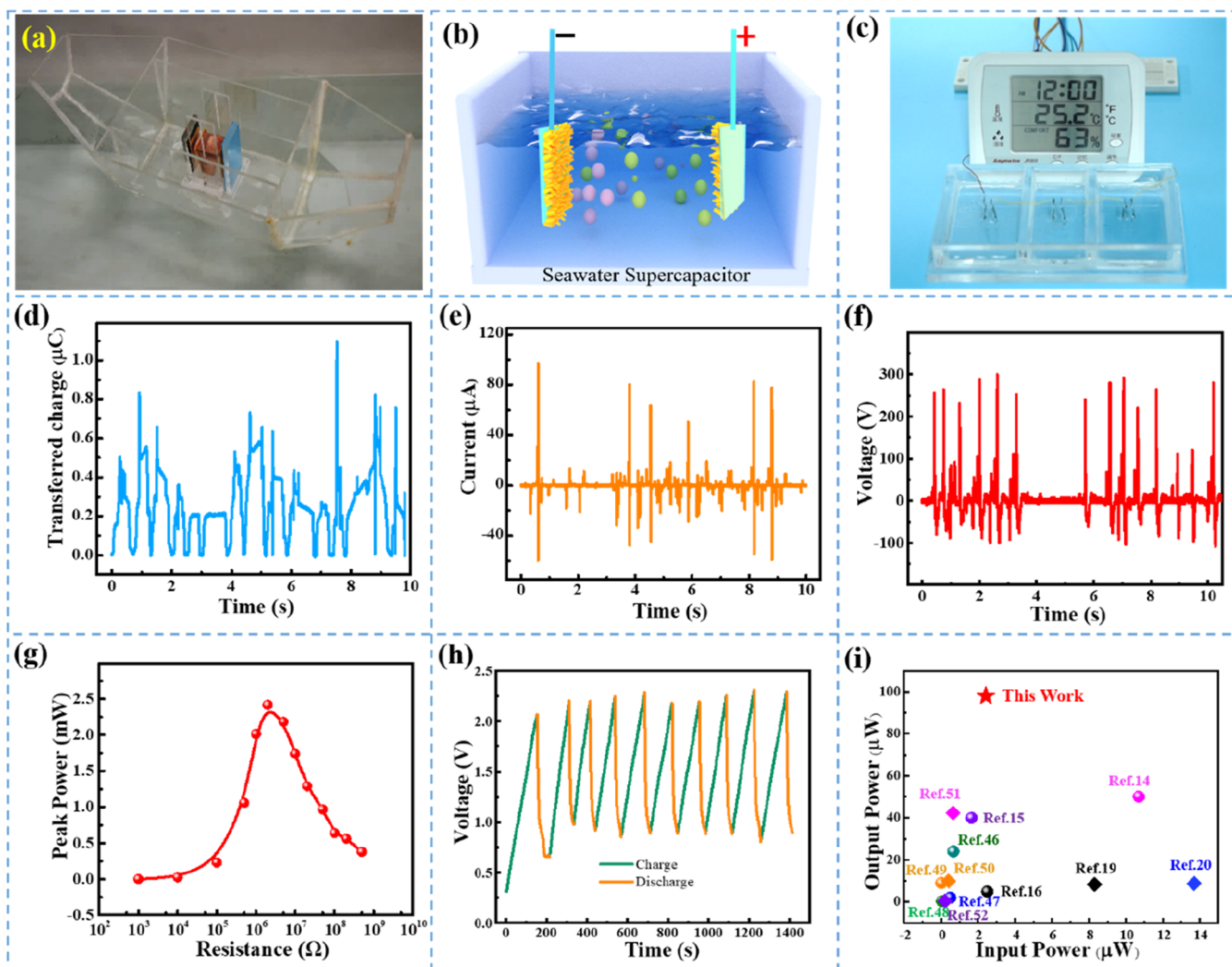


Figure 5. Output performance of the marine self-charging power system in a water wave. The schematic illustration of (a) the TENG module on a boat and (b) SWSCs. (c) Marine self-charging power system drives a hygromograph, (d) transferred charge, and (e) current and (f) voltage of the TENG in the marine self-charging power system in a water wave. (g) Peak power at different load resistances. (h) Stable DC output performance of the marine self-charging power system to charge SWSCs of $150\ \mu\text{F}$ by two M-TENGs for ten cycles and (i) the comparison of the self-charging power system with similar works reported previously.

There is no new compound generated, which is supported by the OM images, XRD tests, and mass retention (Figure S10) after immersing the Ti foil in seawater for 180 days. Thus, a slight increase in the charge transfer and diffusion resistances may be due to the ions and water of the seawater intercalating into the PPy layers as well as the adsorption of foreign ions on the active materials. The conductivities of the seawater electrolyte, PPy film, and the PPy film after 180 days in seawater are 0.051, 190.3, and $73.5\ \text{S cm}^{-1}$, respectively, further suggesting that the embedding of seawater into PPy would increase the resistance. The CV curves (Figure 3h) and the GCD tests (Figure 3i) further suggest that even after the immersion in seawater for 180 days, the assembled SWSC presents the same stability.

Electrochemical Performances of h-PPy SWSCs in Series. In order to satisfy the energy demands for practical applications, several SWSCs are integrated into assemblies in series (Figure 4a). The EIS suggests that although SC units increase from one to three, the inherent resistance (R_1) and the charge transfer resistance (R_{ct}) are 2.0, 3.5, and 5.9 and 3.5, 12.5, and $29.7\ \Omega$, respectively (Figure 4b). Also, the h-PPy SCs

in the series still exhibit a typical capacitive property (Figure 4c). CV curves show that the output voltage of the h-PPy SCs in the series increases linearly with the increase in h-PPy SC units. Moreover, the SWSC still acquires a fast charging/discharging ability at a high scan rate of $200\ \text{mV s}^{-1}$ when two SCs and three SCs are in series at a high scan rate of $200\ \text{mV s}^{-1}$ (Figure 4d,e). The results are also supported by the GCD tests, which show symmetric and linear curves in the entire range of potential (0–2.4 V) (Figure 4f). The specific capacitance of the SWSCs in the series with different numbers of units (1–3) (Figure 4i) obtained from the GCD tests (Figure 4g,h) shows that the as-prepared SCs with PPy as electrodes and natural seawater as the electrolyte have tunable adaptability and reliable scalability to store the blue energy harvested by TENG *in situ*.

Output Performances of the Marine Self-Charging Power System in a Water Wave. The output performance of the marine self-charging power system was first studied using a linear motor in Figure S12. The assembled TENG module can achieve $\sim 200\ \text{W m}^{-3}$ ($98.4\ \text{W m}^{-3}$ for each M-TENG) when driven by a linear motor with the transferred

charges, short current, and open voltage of M-TENG at 1.42 μC , 147 μA , and 584 V, respectively. The designed TENG outperforms the marine TENG reported to date, including the spherical TENG,^{14,46} arc-shaped TENG,¹⁵ cylindrical TENG-EMG hybrid device,¹⁸ tubular TENG,² water balloon TENG,¹⁶ stacked pendulum-structured TENG,¹⁷ and stacked pendulum-structured TENG³⁵ as shown in Table S2. In addition, when the motor acceleration is 1, 3, and 5 m s^{-2} , the M-TENG can take 145, 118, and 88.5 s to raise the voltage of the seawater capacitor to 2 V, respectively (Figure S12g). This result fully verifies the feasibility of using the seawater SC to store the blue energy harvested by TENG *in situ*.

To demonstrate the application of the SWSC for *in situ* energy storage of blue energy harvested by TENG, a water tank is used to simulate water and drive a boat with an integrated TENG module to harvest water wave energy (Figure 5a) and as-prepared h-PPy SWSCs with natural seawater are utilized to store the harvested water wave energy (Figure 5b). It suggests that the SWSC can store the harvested water wave energy by the TENG module and then drive a hygrothermograph (Figure 5c and Movie S1) according to the circuit diagram depicted in Figure S13.

The transferred charge, current, and voltage of the TENG by the driving of the simulative water wave can reach 0.8 μC , 80 μA , and 290 V, respectively (Figure 5d–f). In addition, it is easy to find that the relative maximum peak power of TENG at 2.43 mW can be achieved in the simulative water wave when the external load resistance comes to 2 $\text{M}\Omega$ (Figure 5g).

It suggests that the h-PPy SWSCs in the marine self-charging power system (Figure S14) can be charged to 0.85 and 1.72 V within 150 s by one M-TENG and two M-TENGs, respectively (Figure S15). However, the system takes almost the same time (100 s) to discharge from 2.0 to 0 V under different constant currents (2 μA , 5 μA , and 10 μA) (Figure S16). By using the circuit diagram in Figure S13 to power the external device, the marine self-charging power system exhibits an output power density of 98 μW in the water wave (Figures 5h & S17), which is capable enough to drive the hygrothermograph shown in Figure 5c.

The input from the TENG to SWSC and the output from the self-charging power system are critical parameters that determine the capacity of the self-charging power system to drive the electronics effectively. Owing to the high performance of the SWSC (Figure 5i), the as-prepared self-charging power system delivers a higher power output than the reported work that collects water wave energy.^{14–16,46–48} In addition, even when compared with other forms of energy harvesters, the fabricated self-charging power system exhibits a competitive output.^{19,20,49–52} This study shows that the designed marine self-charging power system is a promising candidate for driving the sensors and devices in the smart ocean and marine IoTs.^{53–56}

CONCLUSIONS

In summary, this paper proposes a marine self-charging power system consisting of the SWSC and TENG to provide a constant DC output for the electronics. SWSCs are used with PPy as electrodes and seawater as the eco-friendly aqueous electrolyte to *in situ* store the water wave energy from TENG. By electrochemical preparation, the h-PPy electrode constructs a continuous uniform film to obtain higher conductivity and avoid the addition of a binder and a conductive agent, which presents a high specific capacitance of 257 F g^{-1} under the

current density of 1 A g^{-1} with the apparent diffusion coefficient of $9.25 \times 10^{-9} \text{ cm}^2 \text{ s}^{-1}$. With the hollow morphology design, the h-PPy electrode can facilitate the ions of seawater transport into active materials and the SWSC achieves a high power density of 4.32 kW kg^{-1} at an energy density of 5.12 W h kg^{-1} . Even after 180 days of aging in seawater, h-PPy still endows weight maintenance of 99.9%, enabling the SWSC to maintain stability of about 99.3% after 6000 cycles. More importantly, when combined with a TENG module to harvest wave energy as the marine self-charging power system, the marine self-charging power system *in situ* stores the electricity from TENG and provides a DC output to drive electronics and sensors, which shows a competitive potential in the smart ocean and IoTs.

METHODS

Preparation of the h-PPy Seawater SC. First, the h-PPy electrode is electrochemically deposited as follows: 400 sodium *p*-toluenesulfonic (TOSNa, CP), 100 mM TOSH (AR), and 300 mM pyrrole (Py, Capchem, 99%) are mixed together by severely stirring under an ice bath. Then, a three-electrode cell composed of titanium sheets as both the counter electrode and working electrode and SCE as the reference electrode is employed for electrodeposition with the pulse potentiostatic method using a versatile multichannel potentiostat 2/Z (VMP2, BioLogic). The mass of the obtained PPy is roughly 0.40 mg.

Second, the as-prepared PPy electrodes are served as both the working electrode and counter electrode, with natural seawater as the electrolyte to assemble the h-PPy seawater SC. Natural seawater is purchased from the Yellow Sea near Qingdao, Shandong province, China. The collected seawater is used without further treatment, with $\text{pH} = 8.28$.

Fabrication of TENG. The design of the TENG used in the article includes three parts: the fabrication of M-TENG, the bifilar-pendulum, and the boat. (1) The fabrication of M-TENG: first, the Kapton film with a thickness of 50 μm is bent into a zigzag structure with each interval of 6.5 $\text{cm} \times 3.6 \text{ cm}$ as the substrate for BM-TENG. Then, the copper foil (3 $\text{cm} \times 5 \text{ cm}$) on the foam film (3.5 $\text{cm} \times 5.5 \text{ cm} \times 50 \mu\text{m}$) and the copper foil (3 $\text{cm} \times 5 \text{ cm}$) covered with the FEP film (3 $\text{cm} \times 5 \text{ cm} \times 100 \mu\text{m}$) are attached at the intervals alternately. (2) The fabrication of the bifilar-pendulum: a copper pendulum with a trapezoid column [2.0 cm (top) \times 4.0 cm (bottom) \times 5.5 cm (height in tread) \times 3.5 cm (height of the column)] is placed in the cubic acrylic box by a fishing line with a diameter of 1 mm. Then, fabricated M-TENG is attached to the bifilar-pendulum. (3) The fabrication of the boat: the boat is fabricated with an acrylic sheet. Typically, acrylic sheets with a thickness of 5 mm are fixed to form the keel of the boat. Based on this, a boat with the size of 50 $\text{cm} \times 20 \text{ cm} \times 30 \text{ cm}$ is built. To ensure the lateral stability of the boat and eliminate the influence of transverse water waves, a pair of acrylic blocks measuring 20 $\text{cm} \times 10 \text{ cm}$ are symmetrically added on both sides of the hull.

Fabrication of the Marine Self-Charging Power System. The marine self-charging power system is composed of a bifilar-pendulum-assisted multilayer-structured triboelectric nanogenerator (BM-TENG) module and a horn-like polypyrrole SC (h-PPy SC) with natural seawater as an electrolyte with a rectifier.

Characterization and Measurement of the Marine Self-Charging Power System. The morphologies of the as-prepared PPy films are characterized with a scanning electron microscope (Hitachi model TM3000) and a transmission electron microscope (TEM, JEOL JEM-2100). The electrochemical performances of the as-prepared PPy are conducted by using a versatile multichannel potentiostat 2/Z (VMP2, BioLogic) in a three-electrode system, where the as-prepared PPy, a platinum foil, and SCE serve as the working electrode, counter electrode, and reference electrode, respectively, and in a two-electrode system where the as-prepared PPy serves as the working electrode and counter electrode. All the

tests are in natural seawater at room temperature. A linear motor (TSMV120-1S) and a seesaw are utilized to drive BM-TENG, and a 2.7 m × 0.7 m × 0.7 m water tank is used to simulate the wave (the water waves are generated by a wave board with periodic motion). The simulated water wave frequency is in the range of 0.2–1 Hz, and the wave height is in the range of 0–20 cm. The programmable electrometer (Keithley model 6514) is applied to test the transferred charges and short-circuit current. The mixed-domain oscilloscope (MDO3024) is utilized to test the open-circuit voltage. A potentiostat (BioLogic, VMP3) is utilized to test the voltage of the capacitor in the charging capacitor test.

■ ASSOCIATED CONTENT

SI Supporting Information

The Supporting Information is available free of charge at <https://pubs.acs.org/doi/10.1021/acsami.1c22129>.

Hygrothermograph driven by the self-charging power system (MP4)

Comparison table for the SWSC; comparison table for the marine-TENGs; schematic illustration of TENG modules; electric potential distribution of the M-TENG unit in different states by COMSOL simulation; bode plot of the h-PPy in a three-electrode system; potential window test from CV at a scan rate of 10 mV s⁻¹ in a three-electrode system with seawater as the electrolyte; CV curves of the as-prepared h-PPy electrode at different scan rates in a three-electrode system with seawater as the electrolyte; SEM image and diffusion coefficient of the conventional cauliflower-like PPy; GCD curve of the h-PPy electrode in a three-electrode system with seawater as the electrolyte; Nyquist impedance and Bode plot of the h-PPy in seawater SC; GCV curves of the h-PPy SCs in a two-electrode system in seawater; stability test in seawater; pH changes of the electrolyte after 180 days; output performance of the BM-TENG module driven by linear motor; circuit diagram showing that the SWSC can store the harvested water wave energy by TENG module and then drive a hygrothermograph; mechanism of SCPS in the revised article with the real-time image of the device; stable DC output performance of the marine self-charging power system to charge the SWSCs of 150 μF by one M-TENG and two M-TENGs; self-charge and constant current discharge for the self-charging power system; and output of marine self-powered system in a water wave (PDF)

■ AUTHOR INFORMATION

Corresponding Author

Jie Wang – Beijing Institute of Nanoenergy and Nanosystems, Chinese Academy of Sciences, Beijing 100083, P. R. China; College of Nanoscience and Technology, University of Chinese Academy of Sciences, Beijing 100049, P. R. China; Center on Nanoenergy Research, School of Physical Science and Technology, Guangxi University, Nanning 530004, P. R. China; orcid.org/0000-0003-4470-6171; Email: wangjie@binn.cas.cn

Authors

Baofeng Zhang – Beijing Institute of Nanoenergy and Nanosystems, Chinese Academy of Sciences, Beijing 100083, P. R. China; College of Nanoscience and Technology, University of Chinese Academy of Sciences, Beijing 100049, P. R. China

Chuguo Zhang – Beijing Institute of Nanoenergy and Nanosystems, Chinese Academy of Sciences, Beijing 100083, P. R. China; College of Nanoscience and Technology, University of Chinese Academy of Sciences, Beijing 100049, P. R. China

Wei Yuan – Beijing Institute of Nanoenergy and Nanosystems, Chinese Academy of Sciences, Beijing 100083, P. R. China; College of Nanoscience and Technology, University of Chinese Academy of Sciences, Beijing 100049, P. R. China

Ou Yang – Beijing Institute of Nanoenergy and Nanosystems, Chinese Academy of Sciences, Beijing 100083, P. R. China; College of Nanoscience and Technology, University of Chinese Academy of Sciences, Beijing 100049, P. R. China

Yuebo Liu – Beijing Institute of Nanoenergy and Nanosystems, Chinese Academy of Sciences, Beijing 100083, P. R. China; Center on Nanoenergy Research, School of Physical Science and Technology, Guangxi University, Nanning 530004, P. R. China

Lixia He – Beijing Institute of Nanoenergy and Nanosystems, Chinese Academy of Sciences, Beijing 100083, P. R. China; College of Nanoscience and Technology, University of Chinese Academy of Sciences, Beijing 100049, P. R. China

Yuexiao Hu – Beijing Institute of Nanoenergy and Nanosystems, Chinese Academy of Sciences, Beijing 100083, P. R. China; Center on Nanoenergy Research, School of Physical Science and Technology, Guangxi University, Nanning 530004, P. R. China

Linglin Zhou – Beijing Institute of Nanoenergy and Nanosystems, Chinese Academy of Sciences, Beijing 100083, P. R. China; College of Nanoscience and Technology, University of Chinese Academy of Sciences, Beijing 100049, P. R. China

Zhong Lin Wang – Beijing Institute of Nanoenergy and Nanosystems, Chinese Academy of Sciences, Beijing 100083, P. R. China; School of Materials Science and Engineering, Georgia Institute of Technology, Atlanta, Georgia 30332, United States; orcid.org/0000-0002-5530-0380

Complete contact information is available at: <https://pubs.acs.org/doi/10.1021/acsami.1c22129>

Author Contributions

B.Z., C.Z. and W.Y. contributed equally to this work.

Notes

The authors declare no competing financial interest.

■ ACKNOWLEDGMENTS

Research is supported by the National Natural Science Foundation of China (grant nos. 61774016, 21773009, and 22109013), the Fundamental Research Funds for the Central Universities (E1E46802), National Key R & D Project from Minister of Science and Technology (2016YFA0202704), the China Postdoctoral Science Foundation (2019M660587), and the Beijing Municipal Science & Technology Commission (Z171100000317001, Z171100002017017, and Y3993113DF).

■ REFERENCES

- (1) Pang, K.; Song, X.; Xu, Z.; Liu, X.; Liu, Y.; Zhong, L.; Peng, Y.; Wang, J.; Zhou, J.; Meng, F.; Wang, J.; Gao, C. Hydroplastic foaming of graphene aerogels and artificially intelligent tactile sensors. *Sci. Adv.* **2020**, *6*, No. eabd4045.
- (2) Zhang, C.; Liu, L.; Zhou, L.; Yin, X.; Wei, X.; Hu, Y.; Liu, Y.; Chen, S.; Wang, J.; Wang, Z. L. Self-Powered Sensor for Quantifying

Ocean Surface Water Waves Based on Triboelectric Nanogenerator. *ACS Nano* **2020**, *14*, 7092–7100.

(3) Liu, S.; Liu, X.; Zhou, G.; Qin, F.; Jing, M.; Li, L.; Song, W.; Sun, Z. A High-Efficiency Bioinspired Photoelectric-Electromechanical Integrated Nanogenerator. *Nat. Commun.* **2020**, *11*, 6158.

(4) Luo, J.; Wang, Z. L. Recent Advances in Triboelectric Nanogenerator Based Self-Charging Power Systems. *Energy Storage Mater.* **2019**, *23*, 617–628.

(5) Pu, X.; Guo, H.; Chen, J.; Wang, X.; Xi, Y.; Hu, C.; Wang, Z. L. Eye Motion Triggered Self-Powered Mechnosensational Communication System Using Triboelectric Nanogenerator. *Sci. Adv.* **2017**, *3*, No. e1700694.

(6) Zi, Y.; Guo, H.; Wen, Z.; Yeh, M.-H.; Hu, C.; Wang, Z. L. Harvesting Low-Frequency (< 5 Hz) Irregular Mechanical Energy: A Possible Killer Application of Triboelectric Nanogenerator. *ACS Nano* **2016**, *10*, 4797–4805.

(7) Zhang, C.; He, L.; Zhou, L.; Yang, O.; Yuan, W.; Wei, X.; Liu, Y.; Lu, L.; Wang, J.; Wang, Z. L. Active Resonance Triboelectric Nanogenerator for Harvesting Omnidirectional Water-Wave Energy. *Joule* **2021**, *5*, 1613–1623.

(8) Liu, W.; Wang, Z.; Wang, G.; Liu, G.; Chen, J.; Pu, X.; Xi, Y.; Wang, X.; Guo, H.; Hu, C.; Wang, Z. L. Integrated Charge Excitation Triboelectric Nanogenerator. *Nat. Commun.* **2019**, *10*, 1426.

(9) Niu, S.; Wang, S.; Lin, L.; Liu, Y.; Zhou, Y. S.; Hu, Y.; Wang, Z. L. Theoretical Study of Contact-Mode Triboelectric Nanogenerators as an Effective Power Source. *Energy Environ. Sci.* **2013**, *6*, 3576–3583.

(10) Wu, C.; Wang, A. C.; Ding, W.; Guo, H.; Wang, Z. L. Triboelectric Nanogenerator: A Foundation of the Energy for the New Era. *Adv. Energy Mater.* **2019**, *9*, 1802906.

(11) Guo, H.; Chen, J.; Wang, L.; Wang, A. C.; Li, Y.; An, C.; He, J.-H.; Hu, C.; Hsiao, V. K. S.; Wang, Z. L. A Highly Efficient Triboelectric Negative Air Ion Generator. *Nat. Sustain.* **2021**, *4*, 147–153.

(12) Huang, C.; Chen, G.; Nashalian, A.; Chen, J. Advances in Self-Powered Chemical Sensing via a Triboelectric Nanogenerator. *Nanoscale* **2021**, *13*, 2065–2081.

(13) He, W.; Liu, W.; Chen, J.; Wang, Z.; Liu, Y.; Pu, X.; Yang, H.; Tang, Q.; Yang, H.; Guo, H.; Hu, C. Boosting Output Performance of Sliding Mode Triboelectric Nanogenerator by Charge Space-Accumulation Effect. *Nat. Commun.* **2020**, *11*, 4277.

(14) Yuan, Z.; Wang, C.; Xi, J.; Han, X.; Li, J.; Han, S.-T.; Gao, W.; Pan, C. Spherical Triboelectric Nanogenerator with Dense Point Contacts for Harvesting Multidirectional Water Wave and Vibration Energy. *ACS Energy Lett.* **2021**, *6*, 2809–2816.

(15) Ren, J.; Gao, C.; An, J.; Liu, Q.; Wang, J.; Jiang, T.; Wang, Z. L. Arc-Shaped Triboelectric Nanogenerator Based on Rolling Structure for Harvesting Low-Frequency Water Wave Energy. *Adv. Mater. Technol.* **2021**, *6*, 2100359.

(16) Xia, K.; Fu, J.; Xu, Z. Multiple-Frequency High-Output Triboelectric Nanogenerator Based on a Water Balloon for All-Weather Water Wave Energy Harvesting. *Adv. Energy Mater.* **2020**, *10*, 2000426.

(17) Zhong, W.; Xu, L.; Wang, H.; Li, D.; Wang, Z. L. Stacked Pendulum-Structured Triboelectric Nanogenerators for Effectively Harvesting Low-Frequency Water Wave Energy. *Nano Energy* **2019**, *66*, 104108.

(18) Feng, Y.; Liang, X.; An, J.; Jiang, T.; Wang, Z. L. Soft-Contact Cylindrical Triboelectric-Electromagnetic Hybrid Nanogenerator Based on Swing Structure for Ultra-Low Frequency Water Wave Energy Harvesting. *Nano Energy* **2021**, *81*, 105625.

(19) Yong, S.; Wang, J.; Yang, L.; Wang, H.; Luo, H.; Liao, R.; Wang, Z. L. Auto-Switching Self-Powered System for Efficient Broad-Band Wind Energy Harvesting Based on Dual-Rotation Shaft Triboelectric Nanogenerator. *Adv. Energy Mater.* **2021**, *11*, 2101194.

(20) Yang, Z.; Yang, Y. Y.; Wang, H.; Liu, F.; Lu, Y. J.; Ji, L. H.; Wang, Z. L.; Cheng, J. Charge Pumping for Sliding-Mode Triboelectric Nanogenerator with Voltage Stabilization and Boosted Current. *Adv. Energy Mater.* **2021**, 2101147.

(21) Su, Y.; Chen, G.; Chen, C.; Gong, Q.; Xie, G.; Yao, M.; Tai, H.; Jiang, Y.; Chen, J. Self-Powered Respiration Monitoring Enabled By a Triboelectric Nanogenerator. *Adv. Mater.* **2021**, *33*, 2101262.

(22) Challagulla, N. V.; Vijayakumar, M.; Sri Rohita, D.; Elsa, G.; Bharathi Sankar, A.; Narasinga Rao, T.; Karthik, M. Hierarchical Activated Carbon Fibers as a Sustainable Electrode and Natural Seawater as a Sustainable Electrolyte for High-Performance Supercapacitor. *Energy Technol.* **2020**, *8*, 2000417.

(23) Zhang, B.; Xu, Y.; Wang, J.; Ma, X.; Hou, W.; Xue, X. Electrochemical Performance of LiFePO₄/Graphene Composites at Low Temperature Affected by Preparation Technology. *Electrochim. Acta* **2021**, *368*, 137575.

(24) Zhang, B.; Xu, Y.; Wang, J.; Lin, J.; Wang, C.; Chen, Y. Lanthanum and Cerium Co-doped LiFePO₄: Morphology, Electrochemical Performance and Kinetic Study from-30-+50 Degrees C. *Electrochim. Acta* **2019**, *322*, 134686.

(25) Chen, L.; Xu, X.; Wan, L.; Zhu, G.; Li, Y.; Lu, T.; Albaqami, M. D.; Pan, L.; Yamauchi, Y. Carbon-Incorporated Fe₃O₄ Nanoflakes: High-Performance Faradaic Materials for Hybrid Capacitive Deionization and Supercapacitors. *Mater. Chem. Front.* **2021**, *5*, 3480–3488.

(26) Han, L.; Huang, H.; Fu, X.; Li, J.; Yang, Z.; Liu, X.; Pan, L.; Xu, M. A Flexible, High-Voltage and Safe Zwitterionic Natural Polymer Hydrogel Electrolyte for High-Energy-Density Zinc-Ion Hybrid Supercapacitor. *Chem. Eng. J.* **2020**, *392*, 123733.

(27) Xu, X.; Tang, J.; Qian, H.; Hou, S.; Bando, Y.; Hossain, M. S. A.; Pan, L.; Yamauchi, Y. Three-Dimensional Networked Metal-Organic Frameworks with Conductive Polypyrrole Tubes for Flexible Supercapacitors. *ACS Appl. Mater. Interfaces* **2017**, *9*, 38737–38744.

(28) Shao, Y.; El-Kady, M. F.; Sun, J.; Li, Y.; Zhang, Q.; Zhu, M.; Wang, H.; Dunn, B.; Kaner, R. B. Design and Mechanisms of Asymmetric Supercapacitors. *Chem. Rev.* **2018**, *118*, 9233–9280.

(29) Pakulski, D.; Czepa, W.; Del Buffa, S.; Ciesielski, A.; Samor, P. Atom-Thick Membranes for Water Purification and Blue Energy Harvesting. *Adv. Funct. Mater.* **2020**, *30*, 1902394.

(30) Khan, N.; Kalair, A.; Abas, N.; Haider, A. Review of Ocean Tidal, Wave and Thermal Energy Technologies. *Renewable Sustainable Energy Rev.* **2017**, *72*, 590–604.

(31) Uihlein, A.; Magagna, D. Wave and Tidal Current Energy - a Review of the Current State of Research Beyond Technology. *Renewable Sustainable Energy Rev.* **2016**, *58*, 1070–1081.

(32) He, H.; Xia, Q.; Wang, B.; Wang, L.; Hu, Q.; Zhou, A. Two-Dimensional Vanadium Carbide (V₂C_{Tx}) MXene as Supercapacitor Electrode in Seawater Electrolyte. *Chin. Chem. Lett.* **2020**, *31*, 984–987.

(33) Cheng, S.; Dai, Z.; Fu, J.; Cui, P.; Wei, K.; Zhang, Y.; Wu, Y.; Liu, Y.; Sun, Z.; Shao, Z.; Cui, X.; Su, Q.; Xie, E. Toward Large-Scale Electrochemical Energy Storage in the Marine Environment with a Highly-Extensible "Paper-Like" Seawater Supercapacitor Device. *J. Mater. Chem. A* **2021**, *9*, 622–631.

(34) Zhou, C.; Zhang, Y.; Li, Y.; Liu, J. Construction of High-Capacitance 3D CoO@Polypyrrole Nanowire Array Electrode for Aqueous Asymmetric Supercapacitor. *Nano Lett.* **2013**, *13*, 2078–2085.

(35) Zhang, C.; Zhou, L.; Cheng, P.; Liu, D.; Zhang, C.; Li, X.; Li, S.; Wang, J.; Wang, Z. L. Bifilar-Pendulum-Assisted Multilayer-Structured Triboelectric Nanogenerators for Wave Energy Harvesting. *Adv. Energy Mater.* **2021**, *11*, 2003616.

(36) Tian, W.; Mao, X.; Brown, P.; Rutledge, G. C.; Hatton, T. A. Electrochemically Nanostructured Polyvinylferrocene/Polypyrrole Hybrids with Synergy for Energy Storage. *Adv. Funct. Mater.* **2015**, *25*, 4803–4813.

(37) Torres-Gómez, G.; Tejada-Rosales, E. M.; Gómez-Romero, P. Integration of Hexacyanoferrate as an Active Species in a Molecular Hybrid Material. Transport Properties and Application of Polyaniline/Hexacyanoferrate as a Cathode in Rechargeable Lithium Batteries. *Chem. Mater.* **2001**, *13*, 3693–3697.

(38) Rodríguez, J.; Grande, H.; Otero, T. F.; Trigaud, T.; Moliton, J. P. Implanted Polymer Junctions from Highly Compacted Polypyrrole Films. *Synth. Met.* **1996**, *83*, 201–203.

(39) Park, D. S.; Shim, Y. B.; Park, S. M. Degradation Kinetics of Polypyrrole Films. *J. Electrochem. Soc.* **1993**, *140*, 2749–2752.

(40) Amiri, A.; Chen, Y.; Bee Teng, C.; Naraghi, M. Porous Nitrogen-Doped MXene-Based Electrodes for Capacitive Deionization. *Energy Storage Mater.* **2020**, *25*, 731–739.

(41) Zhang, Y.; Lin, B.; Sun, Y.; Zhang, X.; Yang, H.; Wang, J. Carbon Nanotubes@Metal-Organic Frameworks as Mn-based Symmetrical Supercapacitor Electrodes for Enhanced Charge Storage. *RSC Adv.* **2015**, *5*, 58100–58106.

(42) Cottineau, T.; Toupin, M.; Delahaye, T.; Brousse, T.; Bélanger, D. Nanostructured Transition Metal Oxides for Aqueous Hybrid Electrochemical Supercapacitors. *Appl. Phys. A* **2005**, *82*, 599–606.

(43) Wang, L.; Ouyang, Y.; Jiao, X.; Xia, X.; Lei, W.; Hao, Q. Polyaniline-Assisted Growth of MnO₂ Ultrathin Nanosheets on Graphene and Porous Graphene for Asymmetric Supercapacitor with Enhanced Energy Density. *Chem. Eng. J.* **2018**, *334*, 1–9.

(44) Zhao, P.; Yao, M.; Zhang, Q.; Wang, N.; Hu, W.; Komarneni, S. Electrochemical Behavior of Representative Electrode Materials in Artificial Seawater for Fabricating Supercapacitors. *Electrochim. Acta* **2019**, *318*, 211–219.

(45) Raj, C. J.; Manikandan, R.; Rajesh, M.; Sivakumar, P.; Jung, H.; Das, S. J.; Kim, B. C. Cornhusk Mesoporous Activated Carbon Electrodes and Seawater Electrolyte: The Sustainable Sources for Assembling Retainable Supercapacitor Module. *J. Power Sources* **2021**, *490*, 229518.

(46) Liang, X.; Liu, Z.; Feng, Y.; Han, J.; Li, L.; An, J.; Chen, P.; Jiang, T.; Wang, Z. L. Spherical Triboelectric Nanogenerator Based on Spring-Assisted Swing Structure for Effective Water Wave Energy Harvesting. *Nano Energy* **2021**, *83*, 105836.

(47) Xia, K.; Fu, J. M.; Xu, Z. W. Multiple-Frequency High-Output Triboelectric Nanogenerator Based on a Water Balloon for All-Weather Water Wave Energy Harvesting. *Adv. Energy Mater.* **2020**, *10*, 2000426.

(48) Cheng, P.; Guo, H.; Wen, Z.; Zhang, C.; Yin, X.; Li, X.; Liu, D.; Song, W.; Sun, X.; Wang, J.; Wang, Z. L. Largely Enhanced Triboelectric Nanogenerator for Efficient Harvesting of Water Wave Energy by Soft Contacted Structure. *Nano Energy* **2019**, *57*, 432–439.

(49) Zheng, F.; Sun, Y.; Wei, X.; Chen, J.; Yuan, Z.; Jin, X.; Tao, L.; Wu, Z. A Hybridized Water Wave Energy Harvester with a Swing Magnetic Structure toward Intelligent Fishing Ground. *Nano Energy* **2021**, *90*, 106631.

(50) Lin, Z.; Zhang, B. B.; Xie, Y. Y.; Wu, Z. Y.; Yang, J.; Wang, Z. L. Elastic-Connection and Soft-Contact Triboelectric Nanogenerator with Superior Durability and Efficiency. *Adv. Funct. Mater.* **2021**, *31*, 2105237.

(51) Wen, Z.; Yang, Y. Q.; Sun, N.; Li, G. F.; Liu, Y. N.; Chen, C.; Shi, J. H.; Xie, L. J.; Jiang, H. X.; Bao, D. Q.; Zhuo, Q. Q.; Sun, X. H. A Wrinkled PEDOT:PSS Film Based Stretchable and Transparent Triboelectric Nanogenerator for Wearable Energy Harvesters and Active Motion Sensors. *Adv. Funct. Mater.* **2018**, *28*, 1803684.

(52) Muthu, M.; Pandey, R.; Wang, X.; Chandrasekhar, A.; Palani, I. A.; Singh, V. Enhancement of Triboelectric Nanogenerator Output Performance by Laser 3D-Surface Pattern Method for Energy Harvesting Application. *Nano Energy* **2020**, *78*, 105205.

(53) Zhang, B.; Zhou, P.; Xu, Y.; Lin, J.; Li, H.; Bai, Y.; Zhu, J.; Mao, S.; Wang, J. Gravity-Assisted Synthesis of Micro/Nano-Structured Polypyrrole for Supercapacitors. *Chem. Eng. J.* **2017**, *330*, 1060–1067.

(54) Ma, L.; Wu, R. H.; Patil, A.; Yi, J.; Liu, D.; Fan, X. W.; Sheng, F. F.; Zhang, Y. F.; Liu, S.; Shen, S.; Wang, J.; Wang, Z. L. Acid and Alkali-Resistant Textile Triboelectric Nanogenerator as a Smart Protective Suit for Liquid Energy Harvesting and Self-Powered Monitoring in High-Risk Environments. *Adv. Funct. Mater.* **2021**, *31*, 2102963.

(55) Zhao, L.; Duan, J.; Liu, L.; Wang, J.; Duan, Y.; Vaillant-Roca, L.; Yang, X.; Tang, Q. Boosting Power Conversion Efficiency by Hybrid Triboelectric Nanogenerator/Silicon Tandem Solar Cell Toward Rain Energy Harvesting. *Nano Energy* **2021**, *82*, 105773.

(56) Wang, J.; Yu, X.; Zhao, D.; Yu, Y.; Gao, Q.; Cheng, T. H.; Wang, Z. L. Enhancing Output Performance of Triboelectric

Nanogenerator via Charge Clamping. *Adv. Energy Mater.* **2021**, *11*, 2103056.

JACS Au
AN OPEN ACCESS JOURNAL OF THE AMERICAN CHEMICAL SOCIETY

Editor-in-Chief
Prof. Christopher W. Jones
Georgia Institute of Technology, USA

Open for Submissions

pubs.acs.org/jacsau ACS Publications
Most Trusted. Most Cited. Most Read.